Journal of Polymers and the Environment (2024) 32:3810–3821
https://doi.org/10.1007/s10924-024-03211-x

ORIGINAL PAPER

Degradation Behavior of Poly (Lactic Acid) during Accelerated Photo-Oxidation: Insights into Structural Evolution and Mechanical Properties

Xueping Liu[2] · Xiangdong Hua[1] · Hao Wu[1]

Accepted: 10 February 2024 / Published online: 23 February 2024

Abstract
Poly (lactic acid) (PLA) has received considerable attention as a sustainable and biodegradable alternative to petroleum-based polymers in recent years. In general, the properties of PLA depend on its molecular chain structure, e.g., linear, branched, and aggregated structure, e.g., orthorhombic α-form and stereocomplex crystals. However, the evolution of hierarchical structure triggered by photo-oxidation degradation remain elusive for PLA. Herein, the accelerated photo-oxidation degradation behaviors of PLA samples with different thermal histories, including quenching (PLA-q), slow cooling (PLA-c), and annealing (PLA-a), were investigated by several characterization techniques. Compared to PLA-q and PLA-c, PLA-a exhibits relatively lower rates of molecular chain scission and oxygen-containing groups generation during the accelerated photo-oxidation process, suggesting that the increase in crystallinity contributes to suppressing the degradation of PLA. Changes in the molecular chain structure leads to the evolution of aggregation structure. The crystallinity of PLA samples, whether slowly cooled or annealed, increases with UV exposure time, which is attributed to the newly-formed crystals induced by chemi-crystallization. Unexpectedly, although PLA-a exhibits a slower photo-oxidation degradation rate than PLA-q and PLA-c, it undergoes embrittlement at an earlier stage. Morphological observations of photo-oxidized samples indicate that the degradation reaction of PLA-a occurs preferentially in the amorphous region, transforming the molecular chains into volatile products and eventually resulting in the embrittlement of PLA materials. This research sheds light on photo-oxidation degradation behaviors of PLA, and will serve as a valuable reference for investigating the degradation of other bio-based polymeric materials.

Keywords Polylactic acid · Photo-oxidation Degradation · Aggregation Structure

Introduction

The growing concerns regarding the environmental issues arising from non-degradable petroleum-based polymers have been prominent in recent years [1]. Polylactide (PLA), as one of the leading degradable polymers, is gaining increasing attention among researchers [2, 3]. Compared to traditional petroleum-based plastics, PLA has the following two main advantages. Firstly, PLA is fully degradable under composting conditions without posing a threat to the environment. Secondly, PLA is made from renewable resources such as corn starch, tapioca roots, or sugarcane, resulting in a lower carbon footprint [4, 5]. Furthermore, PLA exhibits excellent processability, as it can be easily processed using conventional plastics processing techniques such as extrusion, injection molding, film blowing, and fiber spinning [6, 7]. To data, however, PLA is primarily used in disposable packaging materials, accounting for over 60% of its usage [8, 9], which does not challenge the dominance of petroleum-based plastics in various fields such as commodity, transport, and agriculture, etc. The inherent shortcomings of PLA, including poor toughness, and relatively lower

✉ Hao Wu
wuhao@qust.edu.cn

[1] Key Laboratory of Rubber-Plastics, Shandong Provincial Key Laboratory of Rubber-Plastics, Ministry of Education, Qingdao University of Science & Technology, Qingdao 266042, China

[2] School of Materials Science and Engineering, Shandong University of Science and Technology, Qingdao 266590, China

heat deflection temperature (HDT), are important bottlenecks that limit its wider applications [10, 11]. Moreover, the biodegradability of PLA renders it more susceptible to photo-oxidation, thermo-oxidation and hydrolytic degradation. The degradation of PLA leads to decrease of molecular weight, change in color, and drastic loss of mechanical properties and use value [12–14]. Therefore, investigating the degradation behavior and mechanisms of PLA is vital to enhance its durability and prolong its service life [15].

Environmental factors including temperature, humidity and light intensity, have a direct impact on the degradation behavior of PLA [16]. The study by Lila et al. [17] showed that the tensile and flexural moduli of PLA increased and then decreased with the increase in thermal-oxidation temperature and time. This is because the initial heat treatment during thermal-oxidation degradation increases the crystallinity and grain size of PLA. Moreover, it was reported by Ndazi et al. [18] that the water absorption and degradation of PLA/rice hulls composites were increased significantly at thermophilic temperatures, because the presence of water vapor can accelerates the hydrolysis of ester groups in the PLA molecular chains, and leading to a rapid reduction in the molecular weight [19]. In outdoor environments, rainwater may contain acids, ionic salts, organic matter, and other substances, all of which can exacerbate the degradation of PLA. In addition to environmental factors, the photo-oxidation degradation characteristics of PLA also depend on its chemical structure and micro-aggregated structural states, among which the influences of molecular weight and crystallinity are most significant. It is generally accepted that low molecular weight PLA has a relatively lower thermal decomposition temperature and is more susceptible to degrade under thermal or humid conditions. The main reason for this phenomenon is that the end groups of PLA molecular chains play a self-catalytic role in the degradation process [20, 21]. In contrast to molecular weight, the influence of crystallinity on the degradation behavior of PLA remains a topic of debate in the literature. While some studies have suggested that increasing crystallinity can reduce the chain segment movement ability of PLA, thereby slowing down the diffusion of oxygen and water molecules and inhibiting degradation [22, 23], others reject this idea. As an example, Tsuji et al. [24] discovered that PLA with higher crystallinity of stereocomplex crystallites is more prone to embrittle during degradation, which is attributed to the preferential destruction of molecular chain segments within the amorphous region caused by photo-oxidation reaction. In general, despite extensive research on the changes in the chemical structure of PLA molecular chains induced by photo-oxidation degradation (e.g., Norrish reactions, crosslinking, and chain scission) [25, 26], a comprehensive physical image describing the evolution of the aggregated state structure is still scarce.

In order to predict the service life of PLA materials and understand the underlying degradation mechanisms, we usually need to conduct degradation experiments under specific conditions. While outdoor weathering tests offer the most reliable data for PLA durability studies, they typically necessitate long experimental periods that can extend to several months [27]. Additionally, the results of environmental weathering experiments are hard to be replicated as they rely on uncontrolled variables, including atypical hot or cold weather, persistent rainfall, and strong winds [28]. In contrast to outdoor weathering tests, accelerated degradation experiments allow the exposure of polymeric materials to simulated conditions that are somehow related to outdoor exposure. By monitoring changes in molecular weight or mechanical properties, or by observing surface deterioration such as discoloration and erosion, the state and extent of degradation can be evaluated in a rationally short period of time, and the key factors that influence the degradation behavior can be precisely assessed [29, 30]. For the photo-oxidation degradation of PLA, the execution of accelerated photo-oxidation experiments on PLA samples with diverse aggregate state structures is anticipated to reveal the degradation-induced microstructural evolution and its corresponding structure-property relationship.

In the present work, the photo-oxidation degradation behaviors of PLA under accelerated UV exposure test are systematically investigated by combining of several characterization techniques including gel permeation chromatography (GPC), Fourier transform infrared spectroscopy (FT-IR), differential scanning calorimetry (DSC), small angle X-ray scattering (SAXS) and atomic force microscopy (AFM). The following aspects are focused: (1) the microstructure evolutions of PLA induced by photo-oxidation, (2) the effects of aggregation structure on photo-oxidation degradation, and (3) the structure-property relationship of photo-oxidized PLA. Based on the obtained results, a comprehensive model is summarized to describe the structure evolution and performance deterioration of PLA film during photo-oxidation, and we believe that this research will be of meaningful reference to the degradation investigation of other bio-based polymeric materials.

Experimental Section

Materials and Sample Preparation

The commercial poly(L-lactide) resin (REVODE 190) used in this study was supplied by Zhejiang Hisun Biomaterials Co., Ltd. The number-average, weight-average

molecular weights (M_n and M_w) and polydispersity index (PDI) of PLLA are 8.4×10^4 g/mol, 21.3×10^4 g/mol and 2.5, respectively.

Prior to the melt processing, the PLA resin was dried at 80 °C in vacuum oven for 12 h to remove water traces. PLA films for photo-oxidation degradation experiments were prepared by compression molding via three different routes, including melt quenching, slow cooling, and annealing after melt quenching, as illustrated in Scheme 1. The obtained PLA films were denoted as PLA-q, PLA-c, and PLA-a, respectively. For PLA-q, the specific preparation process is as follows. PLA pellets were preheated at 200 °C for 3 min and then hot-pressed at 5 MPa and 200 °C by using laboratory-made hydraulic press. After that, the molten film was rapidly immersed into ice-water mixture to obtain a solidified film with thickness of ca. 100 μm. In the case of PLA-a, it can be produced by annealing the quenched PLA film, i.e., by hot pressing the PLA-q film at 120 °C for 15 min. Moreover, the preparation procedure of PLA-c was similar to that of PLA-q except that the molten PLA film and stainless-steel mould were transferred together to another hydraulic press and were cooled at a cooling rate of 10 °C/min. The thickness of PLA-a and PLA-c was also ca. 100 μm.

Photo-Oxidation Degradation Procedure

The accelerated UV degradation tests of PLA-q, PLA-c and PLA-a were carried out in a Scientz03-II ultraviolet cross-linker (SCIENTZ, China) equipped with 5 UV-B lamps (G8T5E, Sankyo-Denki, Japan), which emits ultraviolet rays between 280 and 360 nm (peak at 305-315 nm). It was measured by ultraviolet radiometer (SENTRY ST-513, China) that the light intensity on the lower surface of the UV irradiation chamber was ca. 10 mW/cm^2. PLA films were placed in the middle of the UV irradiation chamber before the accelerated UV degradation test and were taken out from the chamber at an interval of 20 h to investigate the photo-oxidation degradation behaviors.

Characterization

The transmission mode Fourier-transform infrared (FTIR) spectra of photo-oxidized PLA films were collected on a Bruker tensor 27 infrared spectrometer (Bruker, US) in the wavenumber range from 4000 to 600 cm^{-1} with a 4 cm^{-1} resolution. 32 scans were performed for each spectrum at room temperature. To avoid the influence of thickness, the collected FTIR spectra were normalized by the reference band at 2997 cm^{-1} (characteristic band of C-H stretching vibration). The anhydride group content was quantitatively determined by statistically analyzing the height of the spectral bands located at 1845 cm^{-1} (Δ_{1845}) in the FTIR differential spectra. Furthermore, to obtain more detailed chemical structure-related information, PLA samples were dissolved in chloroform and then cast onto potassium bromide (KBr) crystal substrates for transmission mode FTIR measurements. The measurements were conducted with a resolution of 2 cm^{-1} and 32 scans.

Gel permeation chromatography (GPC) analyses were conducted on a Waters GPC equipped with Shodex KD804 column, 515 HPLC pump and 2414 RI detector. DMF was used as the mobile phase at a flow rate of 1 mL/min, and PS standard was used for molecular weight calibration. Samples were dissolved in DMF with concentration of 15 mg/ml before GPC measurements.

Differential scanning calorimetry (DSC) measurements were performed by using a TA Q2000 DSC instrument

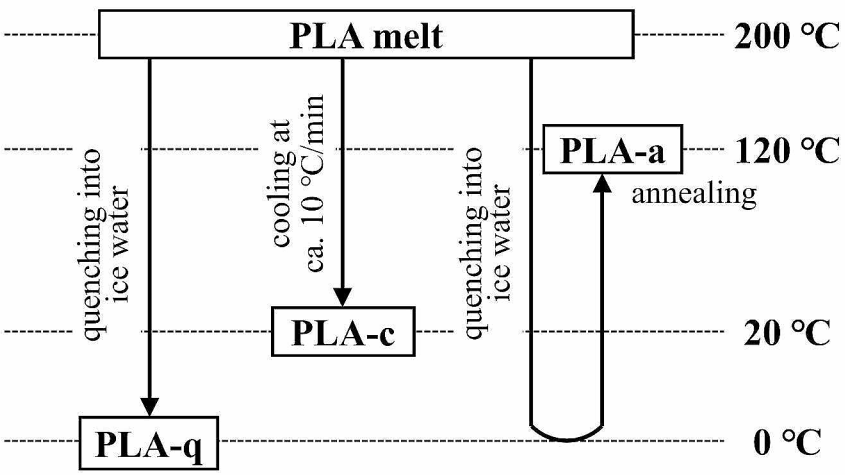

Scheme 1 Preparation procedure of PLA films with different thermal history for accelerated photo-oxidation degradation tests.

under an ultra-high purity nitrogen atmosphere. Samples were heated from 0 to 200 °C at a heating rate of 10 °C/min, held at this temperature for 3 min, then cooled to 0 °C and second heated to 200 °C at a rate of 10 °C/min. The glass transition temperature (T_g), cold crystallization temperature (T_c), cold crystallization enthalpy (ΔH_c), melting temperature (T_m) and melting enthalpy (ΔH_m) of samples were determined from the first heating DSC scans.

Two-dimensional wide-angle X-ray diffraction (2D-WAXD) and small-angle X-ray scattering (2D-SAXS) measurements were carried out on a Xeuss 2.0 h SAXS/WAXS system (Xenocs SA, France) equipped with a multilayer focused Cu Kα X-ray source and a semiconductor detector (Pilatus 300 K, DECTRIS, Switzerland). The distance between sample and detector was 170 and 2500 mm for WAXD and SAXS measurements, respectively. 1D-SAXS and 1D-WAXS curves were obtained by azimuthal integration of the 2D patterns after background subtraction. The crystallinity of samples was determined by peak fitting method, and the long period values of samples were calculated according to Braggs law, $L_P=2\pi/q$, here q is the peak position on 1D scattering curves.

The morphology of exposed surface was characterized by using atomic force microscope (Multimode 8 AFM, Bruker Nano, USA) with Bruker ScanAsyst-Air silicon cantilever tips in the ScanAsyst mode under ambient condition. The resonance frequency and spring constant of tips were 70 kHz and 0.4 N/m, respectively.

Tensile properties were obtained using a Instron 5943 universal test machine. Before tests, PLA films were cut into rectangular samples with length in 30 mm and width in 5 mm and were conditioned at 23 °C and 50% RH (relative humidity) for 24 h. Tensile tests were performed at a crosshead speed of 1 mm/min at room temperature.

Results and Discussion

Effect of Photo-Oxidation Degradation on the Chemical Structure of PLA

FTIR spectroscopy technique is very sensitive to the formation and accumulation of degradation by-products, i.e., hydroperoxides or oxygen-containing functional groups such as carbonyl, anhydride, and carboxyl groups, during polymer degradation, and thus can assess the extent of degradation quantitatively. In the present work, the photo-oxidation induced chemical structure evolution of PLA samples with different thermal history was first investigated by using IR spectroscopy. As shown in Figure S1, the intensity of most absorption bands in the transmission mode FTIR spectra of PLA films exceeds the upper limit of the IR detector because the PLA films are too thick. However, it is hard to identify the absorption bands of degradation products, even with an UV exposure time of 120 h. The main reason for this phenomenon is that most of the degradation products associated with the chain scission contain carbonyl groups, which overlap with the intrinsic PLA carbonyl IR band located in the 1700–1750 cm^{-1} region.

In order to amplify the differences between the spectra, the spectrum of original PLA was subtracted from the spectra of photo-oxidized PLA, and the corresponding difference spectra are illustrated in Fig. 1. It can be found that two positive peaks located at 1845 cm^{-1} and 1648 cm^{-1} appear in the difference spectra, and the intensity of these two peaks increases with the duration of UV exposure. According to the previous reports, the above-mentioned two peaks correspond to anhydride group and vinyl unsaturation group [31, 32], respectively, both of which are associated with the photo-oxidation of PLA. The appearance of the absorption band of anhydride group implies that the photo-oxidation degradation of PLA films in the present work mainly follows a hydroperoxide decomposition mechanism proposed by Bocchini et al. [33]. Several steps, including the formation of peroxide radical and hydroperoxide, the photolysis of hydroperoxide, and the β-scission of alkoxyl radical (PO·) which yields carboxylic group, carbonyl radical, and anhydride group, are involved in this mechanism. On the other hand, the well-known Norrish II degradation reaction mechanism, i.e., the breakage of C-O bond, followed by the formation of hydroxide (OH) group and C = C bond at new terminals, also exists in the photo-oxidation of PLA [34].

Based on the IR results, the variation of the intensity of the spectral band at a wavenumber of 1845 cm^{-1} (Δ_{1845}) with UV exposure time was recorded and plotted in Fig. 1d to visualize the differences in the accumulation of degradation products among various samples. For both PLA-q and PLA-c, the value of Δ_{1845} increases rapidly with the prolongation of time and reaches 0.23 and 0.16, respectively, when the UV exposure time is 120 h. For PLA-a, however, the Δ_{1845} first increases with time and then remains almost constant, which means that the formation of degradation products in PLA-a is somewhat inhibited when the photo-oxidation degradation reaction proceeds to a certain extent.

In addition, conducting transmission mode FTIR measurements directly for PLA film can lead to saturation of the intensity of partial absorption bands. Therefore, we also dissolved the samples in chloroform and cast them onto KBr crystal substrates for FTIR measurements. As shown in Figure S2, the absorption bands located in the infrared fingerprint region are almost unchanged with UV exposure time, indicating that the fundamental chemical structure

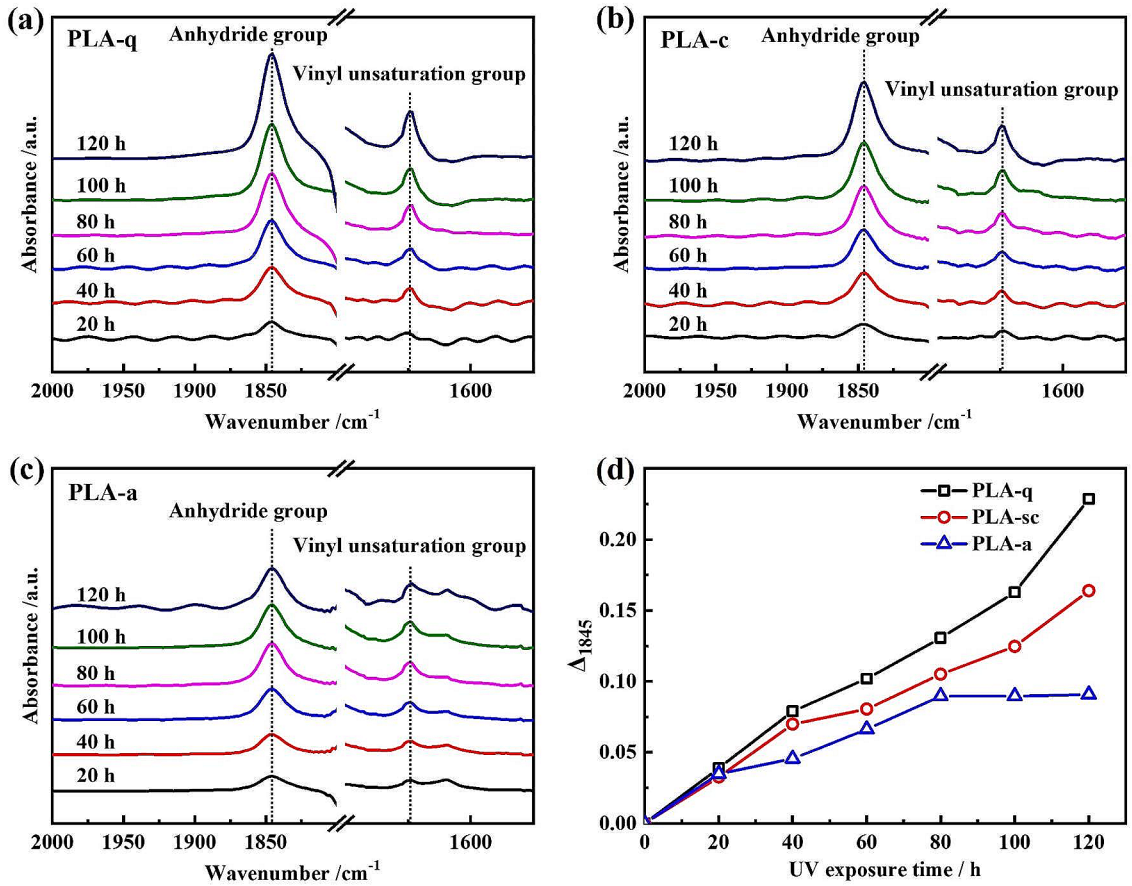

Fig. 1 Subtracted FTIR spectra of photo-oxidized PLA-q (**a**), PLA-c (**b**) and PLA-a (**c**) with different UV exposure times. (**d**) Variation of the intensity of the spectral band at 1845 cm^{-1} (Δ_{1845}) with UV exposure time for PLA-q, PLA-c and PLA-a.

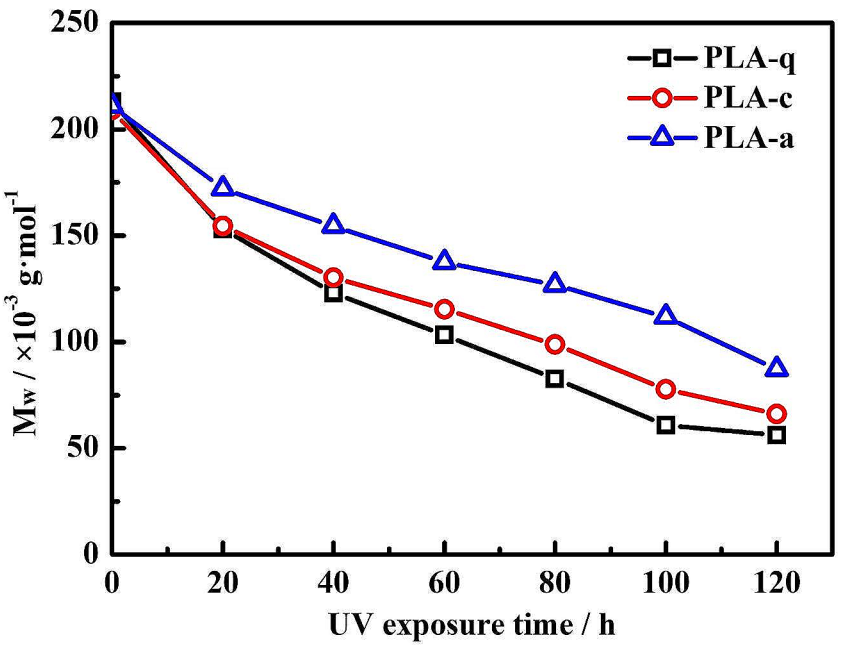

Fig. 2 Evolution of the weight-average molecule weight (M_w) with UV exposure time for PLA-q, PLA-c and PLA-a.

of PLA remains largely unaffected. However, the intensity of the absorption band at 1758 cm^{-1}, corresponding to the carbonyl group in the PLA molecular chain, decreased with prolonged photo-oxidation time, which reflects the cleavage of ester bonds in the molecular chain induced by photo-oxidation degradation. In comparison to PLA-c and PLA-a, the carbonyl absorption bands in the IR spectra of PLA-q exhibits a more pronounced tendency to diminish, indicating a higher probability of molecular chain scission. This analysis is consistent with the GPC results. As illustrated in Fig. 2, the weight-average molecular weight (M_w) of unaged PLA samples is basically the same, all around 2.1×10^4 g/mol, which implies that the PLA film maintains a consistent molecular chain structure before accelerated photo-oxidation tests, i.e., slow cooling or annealing does not lead to the severe thermal degradation of PLA-c and PLA-a. After UV irradiation, the M_w of all three PLA samples decreases with UV exposure time, which is direct evidence for the random chain scission of PLA. Moreover, it can be found that PLA-a exhibits relatively higher M_w when the UV exposure time exceeds 20 h, while the M_w of PLA-q is always the lowest.

Degradation-Induced Microstructural Evolution of PLA

The aggregated state structure of semi-crystalline polymers plays a crucial role in the photo-oxidation degradation behavior [35]. To explore the difference in the initial aggregated state structure of PLA-q, PLA-c and PLA-a, as well as the structural evolution induced by degradation, DSC measurements were conducted on samples with increasing UV exposure time. Several transition processes, including glass translation at ca. 60 °C (the small endothermic peaks originate from the physical aging of amorphous PLA), cold crystallization at ca. 110 °C and melting at ca. 170 °C appear sequentially in the first heating DSC curves (Fig. 3a and c). Based on the obtained DSC curves, the effects of UV exposure on the cold crystallization temperature (T_{cc}) and melt temperature (T_m) are determined and presented in Fig. 3d.

For PLA-q and PLA-c, cold crystallization peaks can be observed during the first heating process, and the T_{cc} of both samples decreases with increasing exposure time when the UV exposure time exceeds 20 h. We believe that the decrease in T_{cc} is related to the molecular weight reduction of PLA caused by photo-oxidative degradation because previous studies have shown that low molecular weight PLA exhibits a relatively higher crystallization rate within a certain range of molecular [36]. Unlike PLA-q and PLA-c, there is no cold crystallization peak in the first heating DSC curves of PLA-a, because it can crystallize adequately during annealing process.

The melting peak of semi-crystalline polymer can provide more information related to the crystal region, including crystal form, crystallinity and lamellar thickness [37]. On can find that the melting peaks of PLA-q and PLA-c shift towards lower temperatures with increasing UV exposure time, and shoulder peaks appear to the left of the main melting peaks. According to the well-accepted Thomson-Gibbs equation [38], the T_m of semi-crystalline polymer depends on the lamellar thickness. Therefore, the reduction in T_m suggests that photo-oxidized PLA-q and PLA-c are less prone to form thick lamellae during the cold crystallization. Combining the IR results that the photo-oxidation

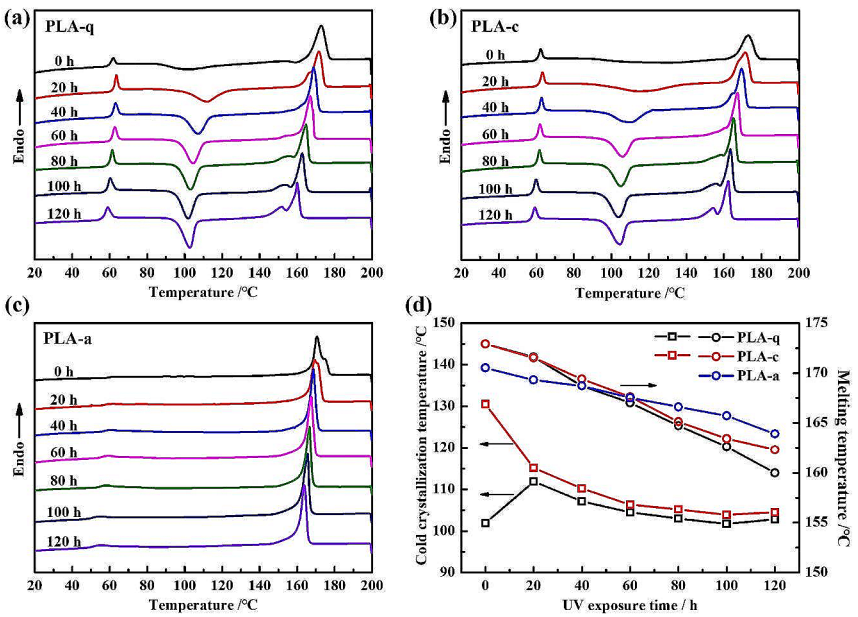

Fig. 3 First heating DSC curves of PLA-q (**a**), PLA-c (**b**) and PLA-a (**c**) with various UV exposure time. (**d**) The effects of UV exposure time on the cold crystallization temperature and melting temperature of photo-oxidized PLA samples

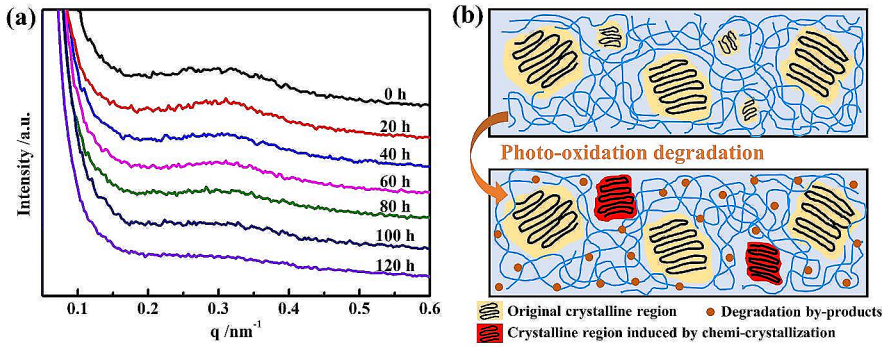

Fig. 4 (**a**) 1D-SAXS curves of unaged and photo-oxidized PLA-a with different UV exposure times. (**b**) Illustration of the microstructural evolution of PLA-a induced by photo-oxidation degradation

degradation of PLA generates carbonyl and anhydride groups, it is believed that the crystallizability of aged PLA is related to the regularity of molecular chains. Specifically, the chemical irregularities generated by photo-oxidation degradation reduce the stereoregularity of PLA molecular chains and accordingly hinder 10_3 helical conformational arrangements, therefore, PLA molecular chains crystallize into relatively thinner lamellae. On the other hand, the photo-oxidation degradation has comparatively less effect on the T_m of PLA-a compared to PLA-q and PLA-c. The T_m of PLA-a is reduced by ca. 6 °C even when the UV exposure time reaches 120 h. This phenomenon suggests that the photo-oxidation degradation occurs mainly in the amorphous region and does not easily destroy the crystalline region of PLA.

The DSC results show that PLA undergoes several phase transition processes such as cold crystallization and melt-recrystallization during heating, which may bring considerable error to the calculation of crystallinity. Consequently, we further performed wide-angle X-ray diffraction (WAXD) measurements for PLA samples with different UV exposure times (Figure S3). The absence of any diffraction peaks in the WAXD curves of PLA-q indicates that all PLA-q samples, either unaged or photo-oxidized, are in amorphous state. In contrast, a small diffraction peak at $2\theta = 16.5°$, originating from the (110/200) plane of α-form crystal of PLA, can be observed in the WAXD curve of unaged PLA-c, suggesting that PLA can crystallize during slow cooling, but with relatively low crystallinity. Moreover, the intensity of the diffraction peaks increase slightly with UV exposure time, which may be due to chemical crystallization caused by photo-oxidation degradation, i.e., the recrystallization of molecular segments released by chain scission [39].

As shown in Figure S3c, the WAXD curve of original PLA-a have several characteristic diffraction peaks at $2\theta = 14.8°$, 16.8°, 19.1° and 22.4°, corresponding to the (010), (200/110), (203) and (015) planes of the orthorhombic α-form crystal of PLA, respectively. The shape of the 1D-WAXD curves remains unchanged upon photo-oxidation degradation, which means that the chemical irregularities induced by degradation do not affect the inherent lattice parameter of PLA crystal. By utilizing the peak-fitting method [40], the crystallinities of unaged and photo-oxidized PLA-a are determined and illustrated in Table S1 and Figure S3d. One can find that the crystallinity gradually increases with UV exposure time. In addition to the chemical crystallization process mentioned above, the erosion of the amorphous region due to photo-oxidation degradation may also be responsible for this phenomenon.

In addition to WAXD, small-angle x-ray scattering (SAXS) was also employed to elucidate the lamellar structure evolution of the crystalline PLA induced by photo-oxidation degradation. As shown in Fig. 4a, a scattering peak can be observed at $q = 0.3$ nm^{-1} in the 1D-SAXS curve of unaged PLA-a. This peak originates from the difference in electron density between crystalline and amorphous regions of PLA, and is commonly regarded as direct evidence of the lamellar structure [9]. As the UV exposure time increases, the intensity of the scattering peak gradually decreases. This result seems confusing, as WAXD analysis indicates that the crystallinity of PLA-a does not decrease, but rather increase after photooxidative degradation. Taking into account the impact of photo-oxidation on the chemical structure of PLA, we believe that the decrease in scattering peak intensity is mainly attributed to the following two factors. Firstly, photo-oxidation degradation induces the generation of oxygen-containing functional groups. Although the amount of oxygen-containing functional groups formed in PLA-a is lower than in PLA-q and PLA-c, most of the functional groups are concentrated in the amorphous region, leading to a reduced difference in electron density between the crystalline and amorphous regions.

Secondly, the newly formed imperfect crystals, which is caused by chemi-crystallization, may not be located on the surface of existing lamellae, but rather within the bulk of amorphous region, as depicted in Fig. 4b. This speculation

can be confirmed by the shift in the position of the scattering peak. One can find that the scattering peak shifts towards higher q value as the photo-oxidation progresses. According to the Braggs law ($L_p=2\pi/q$, where L_p is the long period of two-phase lamellar structure and q is the position of the scattering peak in 1D-SAXS curve), it can be deduced that the L_p decreases with the progress of photo-oxidation [35]. This means that the newly formed crystals occupy a portion of the amorphous region, which in turn reduces the degree of order in the two-phase structure consisting of lamellar and amorphous regions.

Structure-Property Relationship of Photo-Oxidized PLA

The embrittlement induced by random chain scission is a sensitive index for evaluating the degree of degradation in a broad range of degradation processes, including photo-oxidation, thermal oxidation, and hydrolysis [41]. In this study, the tensile properties of photo-oxidized PLA were investigated, Fig. 5a demonstrate the variations in Young's modulus as a function of UV exposure time. Unaged PLA-a exhibits relatively higher Young's modulus (ca. 1.8 GPa) than the other two samples, because molecular chains in crystalline region are densely packed, allowing them to endure the loaded stress. With the prolongation of UV irradiation time, although the crystallinity slightly increases, the Young's modulus of both amorphous and crystalline PLA samples remains almost unchanged.

The elongation at break (ε) of PLA samples with different UV exposure times is plotted in Fig. 5b. The values of ε show a certain dispersion, which is due to the following two factors. Firstly, the samples for tensile tests are PLA films with a thickness of ca. 100 μm. Therefore, stress concentrations are prone to occur during the tensile process. Secondly, PLA itself is brittle, and photo-oxidative degradation may further exacerbate embrittlement. In contrast to the Young's modulus, the elongation at break of PLA undergoes a significant reduction with the increase of UV exposure time, displaying a typical embrittlement phenomenon attributable to photo-oxidation degradation. Notably, the variation of ε induced by degradation is substantially influenced by the aggregation structure of PLA. The initial ε value of PLA-a is 4.3%, obviously lower than that of PLA-q (8.7%) and PLA-c (9.5%). Moreover, PLA-a undergoes embrittlement earlier during photo-oxidation degradation process. When the UV exposure time exceeded 60 h, PLA-a becomes so brittle that it is no longer able to withstand tension test, whereas the other two PLA samples still maintain a certain degree of flexibility.

In general, the degradation-induced embrittlement of polymers is caused by two main factors, the first is the random chain scission, especially the breakage of tie molecular chains interconnecting the lamellae, followed by the formation, growth and propagation of cracks, which is induced by the release of internal stress [42, 43]. For PLA samples with different aggregation structures, the degrees of photo-oxidation degradation and embrittlement are not entirely synchronized. Embrittlement is more prone to occur in PLA-a, although IR and GPC results indicate that this sample has a slower photo-oxidation degradation rate. Combining the above-mentioned structural evolution model (Fig. 4b), we speculated that this phenomenon is related to the preferential occurrence of photo-oxidation reactions in the amorphous region. Specifically, although the degradation rate of crystalline PLA is relatively slow, the breakage of molecular chains and the accumulation of degradation by-products are mostly concentrated in the amorphous region, resulting in a rapid reduction in the number of tie-macromolecules, which in turn leads to a dramatic decrease in the elongation at break.

The preferential occurrence of photo-degradation in the amorphous region of semi-crystalline polymers can be attributed to the following aspects. Firstly, the amorphous regions typically offer greater mobility and accessibility to environmental factors, such as oxygen and UV radiation,

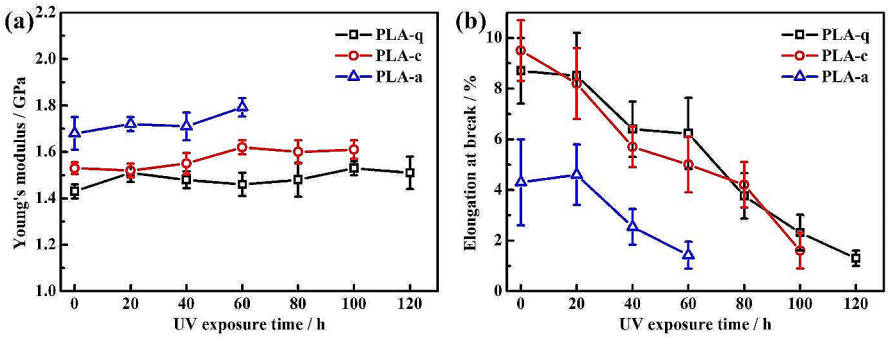

Fig. 5 Evolution of the Young's modulus (**a**) and elongation at break (**b**) with UV exposure time for PLA-q, PLA-c and PLA-a.

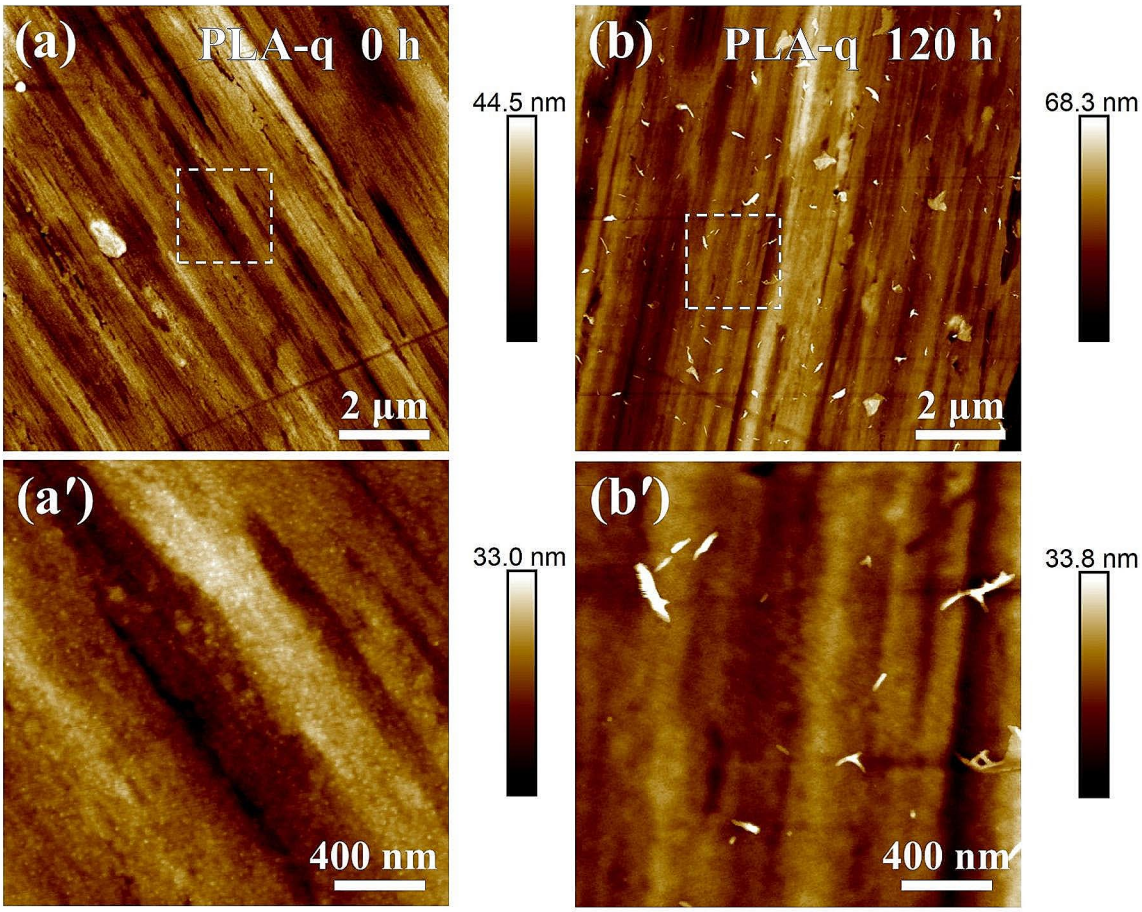

Fig. 6 AFM height images of unaged PLA-q (**a**, **a′**) and photo-oxidized PLA-q with UV exposure time of 120 h (**b**, **b′**)

which can promote degradation processes. Secondly, the amorphous regions often contain more structural defects and chemical impurities, making them more susceptible to degradation reactions. Additionally, the lower packing density and lower degree of order in the amorphous regions make them more prone to the initial attack by photochemical processes. Based on the differences in photo-oxidation degradation behavior among PLA-q, PLA-c, and PLA-a, we believe that controlling the orientation degree through uniaxial or biaxial stretching may be a feasible strategy to improve the durability and service life of PLA films.

To gain deeper insights into the structure-property relationships of photo-oxidized PLA, atomic force microscopy (AFM) was employed to observe the morphology of PLA films. AFM height images of the initial PLA-q and PLA-q with 120 h UV exposure are displayed in Fig. 6a and b, respectively. The surface roughness values determined by AFM are listed in Table S2. Striped morphology appears on the surface of unaged PLA-q, which originates from the polyimide films used during the hot-pressing process. Upon magnifying the selected region (Fig. 6a'), one can find that the sample exhibits a coarse-grained texture, which is basically similar to the surface morphology of other semi-crystalline polymers [30]. When the UV exposure time reaches 120 h, photo-oxidation degradation causes the initial coarse-grained texture to become less prominent (Fig. 6b'), with the surface roughness decreasing from 3.79 nm to 3.14 nm, but no cracks or voids appear on the surface of PLA-q. This phenomenon suggests that the photo-oxidation degradation reaction follows a surface erosion mechanism and occurs uniformly over the entire surface of PLA-q rather than being concentrated in specific areas.

The morphology evolution of PLA-a with UV exposure time is shown in Fig. 7. The surface morphology of unaged PLA-a (Fig. 7a and a′) is generally identical to that of PLA-q, which means that the surface morphology of hot-pressed polymer films mainly depends on the substrates used in the hot-pressing process, rather than the annealing process. With the increase of UV exposure time, lamellar structures gradually appear (Fig. 7b and b′). For the PLA-a irradiated by UV light for 120 h (Fig. 7c and b′), the original striped structures completely disappear, and the exposed lamellae and cracks fill the entire field of view. These results provide direct evidence that the degradation reaction can transform

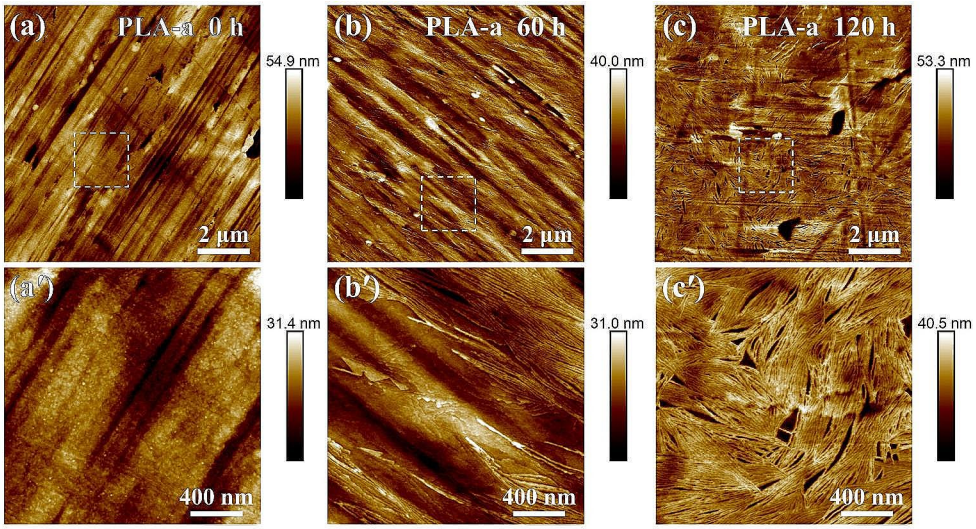

Fig. 7 AFM height images of unaged PLA-a (**a**, **a′**) and photo-oxidized PLA-a with UV exposure time of 60 h (**b**, **b′**) and 120 h (c, c′)

partial molecular chains in the amorphous region into volatile products, which plays a similar role to chemical etching [44].

The morphological characterization allows us to better interpret the variation of mechanical properties of PLA samples with the extent of photo-oxidation degradation. In the case of quenched PLA (PLA-q), despite its faster degradation rate, photo-oxidation degradation does not significantly damage its structure in specific regions. This leads to a gradual decrease in the elongation at break of PLA-q with increasing UV exposure time. On the other hand, for annealed PLA (PLA-a), although the increase in crystallinity due to annealing slows down the overall photo-oxidation degradation rate, the degradation reaction is concentrated in the amorphous region. The reduction in chain scission decreases the number of tie chains, resulting in a rapid decrease in the elongation at break of PLA.

Conclusions

In the present work, the effects of photo-oxidation degradation on the chemical structure, aggregation structure and mechanical properties of PLA are investigated under an accelerated degradation condition. Results reveal that annealed PLA exhibits less degradation by-products accumulation and higher molecular weight compared to quenched and slow cooled PLA samples with same UV exposure time, which indicates that the increase in crystallinity plays a crucial role in suppressing the photo-oxidation degradation of PLA. Furthermore, the changes in the molecular chain structure leads to the evolution of aggregation structure, the photo-oxidation degradation of PLA is accompanied by the re-crystallization of released segments in amorphous region and the erosion of original thick lamellae. Interestingly, despite the fact that annealing reduces the photo-oxidation rate of PLA, annealed PLA undergoes embrittlement at an earlier stage than that of quenched or slow cooled samples. Based on the morphological observations, this phenomenon is thought to be related to the preferential occurrence of degradation reactions in the amorphous region. The degradation transforms the molecular chains into volatile products and eventually resulting in a significant reduction in flexibility.

Supplementary Information The online version contains supplementary material available at https://doi.org/10.1007/s10924-024-03211-x.

Acknowledgements Financial supports from the Shandong Provincial Natural Science Foundation (No. ZR2022QB224), National Natural Science Foundation of China (No. 52203120) and Postdoctoral Innovation Talents Support Program of Shandong Province (No. SDBX2022024) are gratefully acknowledged.

Author Contributions Xueping Liu: Conceptualization, Investigation, Writing - Original Draft. Xiangdong Hua: Formal analysis, Data Curation. Hao Wu: Supervision, Writing - Review & Editing.

Declarations

Competing Interests The authors declare no competing interests.

References

1. Chen GQ, Patel MK (2012) Plastics derived from biological sources: present and future: a technical and environmental review. Chem Rev 112:2082–2099
2. Farah S, Anderson DG, Langer R (2016) Physical and mechanical properties of PLA, and their functions in widespread applications - a comprehensive review. Adv Drug Deliv Rev 107:367–392
3. Inkinen S, Hakkarainen M, Albertsson AC, Sodergard A (2011) From lactic acid to poly(lactic acid) (PLA): characterization and analysis of PLA and its precursors. Biomacromolecules 12:523–532

4. Haider TP, Volker C, Kramm J, Landfester K, Wurm FR (2019) Plastics of the future? The impact of biodegradable polymers on the Environment and on Society. Angew Chem Int Ed Engl 58:50–62
5. Lambert S, Wagner M (2017) Environmental performance of bio-based and biodegradable plastics: the road ahead. Chem Soc Rev 46:6855–6871
6. Lim LT, Auras R, Rubino M (2008) Processing technologies for poly(lactic acid). Prog Polym Sci 33:820–852
7. Jalali A, Romero-Diez S, Nofar M, Park CB (2021) Entirely environment-friendly polylactide composites with outstanding heat resistance and superior mechanical performance fabricated by spunbond technology: exploring the role of nanofibrillated stereocomplex polylactide crystals. Int J Biol Macromol 193:2210–2220
8. Freeland B, McCarthy E, Balakrishnan R, Fahy S, Boland A, Rochfort KD, Dabros M, Marti R, Kelleher SM, Gaughran J (2022) A review of Polylactic Acid as a replacement material for single-use Laboratory Components. Materials 15:2989
9. Jalali A, Huneault MA, Nofar M, Lee PC, Park CB (2019) Effect of branching on flow-induced crystallization of poly (lactic acid). Eur Polym J 119:410–420
10. Mehrabi Mazidi M, Edalat A, Berahman R, Hosseini FS (2018) Highly-toughened Polylactide- (PLA-) based Ternary blends with significantly enhanced Glass Transition and Melt Strength: tailoring the interfacial interactions, phase morphology, and performance. Macromolecules 51:4298–4314
11. Jalali A, Huneault MA, Elkoun S (2016) Effect of thermal history on nucleation and crystallization of poly(lactic acid). J Mater Sci 51:7768–7779
12. Nagarajan V, Mohanty AK, Misra M (2016) Perspective on Polylactic Acid (PLA) based sustainable materials for durable applications: Focus on Toughness and Heat Resistance. ACS Sustainable Chem Eng 4:2899–2916
13. González-López ME, Martín del Campo AS, Robledo-Ortíz JR, Arellano M, Pérez-Fonseca AA (2020) Accelerated weathering of poly(lactic acid) and its biocomposites: a review. Polym Degrad Stab 179:109290
14. Tripathi N, Misra M, Mohanty AK (2021) Durable polylactic acid (PLA)-based sustainable engineered blends and biocomposites: recent developments, challenges, and opportunities. ACS Eng Au 1:7–38
15. Atalay SE, Bezci B, Özdemir B, Göksu YA, Ghanbari A, Jalali A, Nofar M (2021) Thermal and environmentally Induced Degradation behaviors of Amorphous and Semicrystalline PLAs through Rheological Analysis. J Polym Environ 29:3412–3426
16. Zaaba NF, Jaafar M (2020) A review on degradation mechanisms of polylactic acid: Hydrolytic, photodegradative, microbial, and enzymatic degradation. Polym Eng Sci 60:2061–2075
17. Lila MK, Shukla K, Komal UK, Singh I (2019) Accelerated thermal ageing behaviour of bagasse fibers reinforced poly (lactic acid) based biocomposites. Compos Part B: Eng 156:121–127
18. Ndazi BS, Karlsson S (2011) Characterization of hydrolytic degradation of polylactic acid/rice hulls composites in water at different temperatures. Express Polym Lett 5:119–131
19. Copinet A, Bertrand C, Govindin S, Coma V, Couturier Y (2004) Effects of ultraviolet light (315 nm), temperature and relative humidity on the degradation of polylactic acid plastic films. Chemosphere 55:763–773
20. Jamshidi K, Hyon SH, Ikada Y (1988) Thermal characterization of polylactides. Polymer 29:2229–2234
21. Cam D, Marucci M (1997) Influence of residual monomers and metals on poly (l-lactide) thermal stability. Polymer 38:1879–1884
22. Zhou Q, Xanthos M (2008) Nanoclay and crystallinity effects on the hydrolytic degradation of polylactides. Polym Degrad Stab 93:1450–1459
23. Chávez-Montes W, González-Sánchez G, López-Martínez E, de Lira-Gómez P, Ballinas-Casarrubias L, Flores-Gallardo S (2015) Effect of Artificial Weathering on PLA/Nanocomposite Molecular Weight distribution. Polymers 7:760–776
24. Tsuji H, Sugiyama H, Sato Y (2012) Photodegradation of poly(lactic acid) stereocomplex by UV-Irradiation. J Polym Environ 20:706–712
25. Han W, Luo C, Yang Y, Ren J, Xuan H, Ge L (2018) Free-standing polylactic acid/chitosan/molybdenum disulfide films with controllable visible-light photodegradation. Colloid Surf A 558:488–494
26. Hardy C, Kociok-Kohn G, Buchard A (2022) UV degradation of poly(lactic acid) materials through copolymerisation with a sugar-derived cyclic xanthate. Chem Commun 58:5463–5466
27. Lv Y, Huang Y, Yang J, Kong M, Yang H, Zhao J, Li G (2015) Outdoor and accelerated laboratory weathering of polypropylene: a comparison and correlation study. Polym Degrad Stab 112:145–159
28. Pospíšil J, Pilař J, Billingham NC, Marek A, Horák Z, Nešpůrek S (2006) Factors affecting accelerated testing of polymer photostability. Polym Degrad Stab 91:417–422
29. Litauszki K, Kovács Z, Mészáros L, Kmetty Á (2019) Accelerated photodegradation of poly(lactic acid) with weathering test chamber and laser exposure – A comparative study. Polym Test 76:411–419
30. Wu H, Zhao Y, Dong X, Su L, Wang K, Wang D (2021) Probing into the microstructural evolution of isotactic polypropylene during photo-oxidation degradation. Polym Degrad Stab 183:109434
31. Zaidi L, Kaci M, Bruzaud S, Bourmaud A, Grohens Y (2010) Effect of natural weather on the structure and properties of polylactide/Cloisite 30B nanocomposites. Polym Degrad Stab 95:1751–1758
32. Gardette M, Thérias S, Gardette J-L, Murariu M, Dubois P (2011) Photooxidation of polylactide/calcium sulphate composites. Polym Degrad Stab 96:616–623
33. Bocchini S, Fukushima K, Blasio AD, Fina A, Frache A, Geobaldo F (2010) Polylactic acid and polylactic acid-based nanocomposite photooxidation. Biomacromolecules 11:2919–2926
34. Ikada E (1997) Photo- and bio-degradable polyesters. Photodegradation behaviors of aliphatic polyesters. J Photopolym Sci Technol 10:265–270
35. Liu Q, Liu S, Xia L, Hu P, Lv Y, Liu J, Chen Z, Huang Y, Li G (2019) Effect of annealing-induced microstructure on the photo-oxidative degradation behavior of isotactic polypropylene. Polym Degrad Stab 162:180–195
36. Jalali A, Huneault MA, Elkoun S (2017) Effect of molecular weight on the nucleation efficiency of poly(lactic acid) crystalline phases. J Polym Res 24
37. Wu H, Zhao Y, Su L, Wang K, Dong X, Wang D (2021) Markedly improved photo-oxidation stability of α form isotactic polypropylene with nodular morphology. Polym Degrad Stab 189:109595
38. Höhne GWH (2002) Another approach to the Gibbs–Thomson equation and the melting point of polymers and oligomers. Polymer 43:4689–4698
39. Rabello MS, White JR (1997) Crystallization and melting behaviour of photodegraded polypropylene — II. Re-crystallization of degraded molecules. Polymer 38:6389–6399
40. Gao T, Zhang ZM, Li L, Bao RY, Liu ZY, Xie BH, Yang MB, Yang W (2018) Tailoring crystalline morphology by high-efficiency nucleating Fiber: toward high-performance poly(l-lactide) biocomposites. ACS Appl Mater Interfaces 10:20044–20054
41. Fayolle B, Richaud E, Colin X, Verdu J (2008) Review: degradation-induced embrittlement in semi-crystalline polymers having their amorphous phase in rubbery state. J Mater Sci 43:6999–7012
42. Hsu Y-C, Weir MP, Truss RW, Garvey CJ, Nicholson TM, Halley PJ (2012) A fundamental study on photo-oxidative degradation of

linear low density polyethylene films at embrittlement. Polymer 53:2385–2393
43. Croll SG (2022) Stress and embrittlement in organic coatings during general weathering exposure: a review. Prog Org Coat 172:107085
44. Bai H, Huang C, Xiu H, Zhang Q, Fu Q (2014) Enhancing mechanical performance of polylactide by tailoring crystal morphology and lamellae orientation with the aid of nucleating agent. Polymer 55:6924–6934